Team 2 - Executive Summary

MAXINE

VAX TO THE MAX

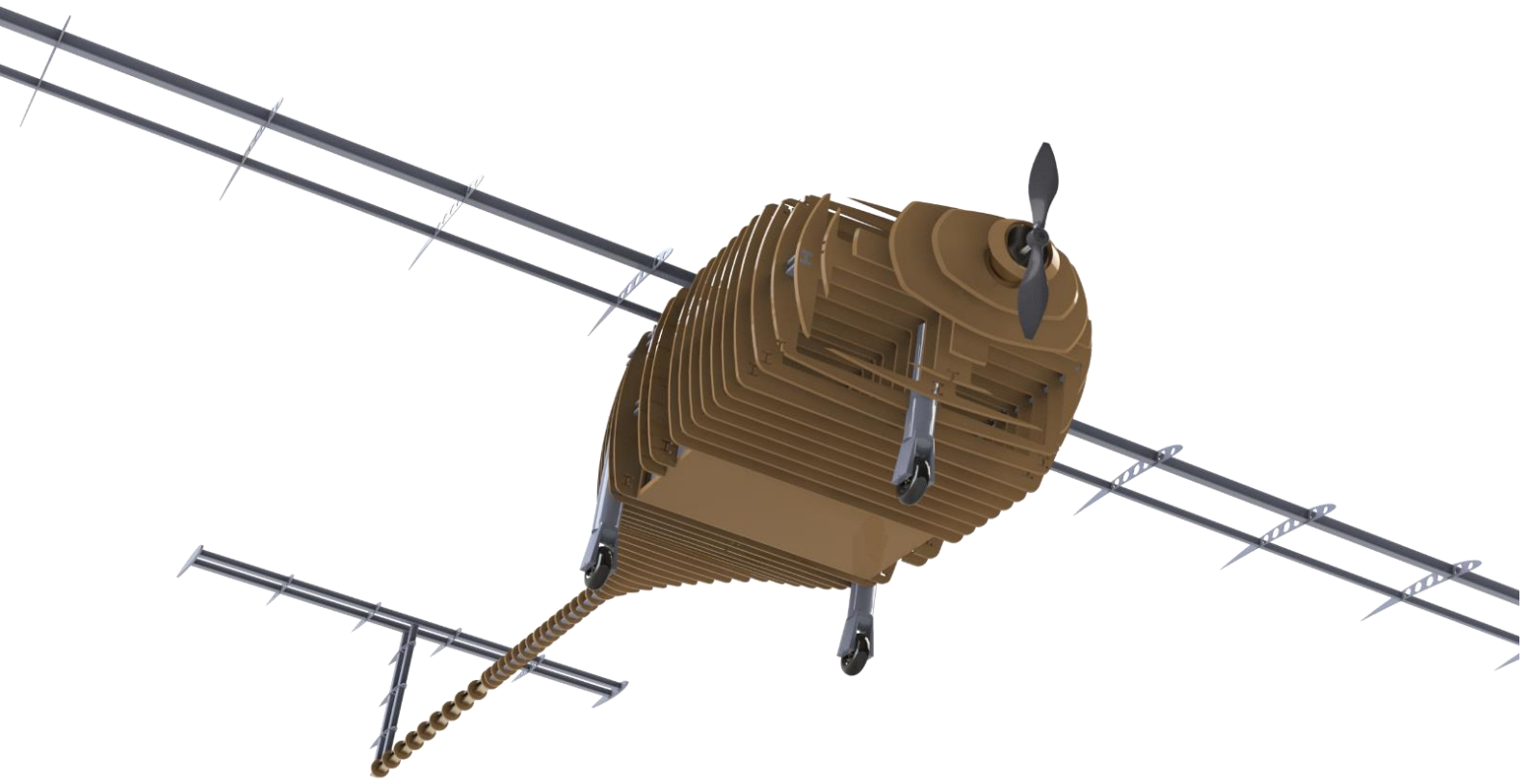

Hadi Alazmi	201349406
Dan Arteni	201330499
Benjamin Cradock	201202928
Luke Eve	201297304
Mark Hawes	201318974
Liam Huckle	201355349
Tanmai Kalathurvadyar	201303308
Joseph Kinirons	201348652
Eduards Maxmacs	201355910
Daniel Nixon	201293466
Alex Salmador	201355097
Alisha Sharma	201301324
Syed Abdullah	201333334
Megan Williamson	201296096

Contents

1 Introduction

To facilitate the fast deployment of vaccines to remote areas as a response to the global pandemic, the MAXINE unmanned aerial vehicle (UAV) has been developed. Following the preliminary design work that was previously completed, which helped to constrain the development process, in-depth and iterative analyses were conducted to ensure compliance with the regulations and demanded mission requirements. This was done through creating the 3D model, which in turn was used in conjunction with results from aerodynamics simulations, under all conditions of flight, in the structural analysis that dictated the material to be used, and in the stability analysis which decided what changes needed to be made to the control surfaces and the fuselage. Finally, the propulsion systems dictated the power supply for both motor and actuators.

2 Mission Specification and Profile

Table 2.1 details the technical specifications required for this mission and whether these specifications are met. The soft specifications are presented by a darker shade.

Table 2.1 - Mission Specification

Specification	Selected Specification	Justification (Section)
Altitude	120m (Hard)	Limited to an altitude of 120m as stated by CAA regulations (A1.1.3) (CAA, 2020).
Range	144km – for a return mission (Hard)	Range achievable by the batteries and deemed acceptable locations
Distance from Operator	72km (Hard)	The range is to be at least double that of the distance from the operator for a return mission. Cellular network and satellite communication (Onslow, 2020)(Abdullah, 2022)
Velocity	50 km/h (min), 120 km/h (max) (Hard)	Maximum and minimum velocities dictated by the V-N structural diagram (Section 6.1.2) (Sharma, 2022)
Mass	19.2kg (Hard)	Internal and structural component total mass (Section 5.2)
Payload	3kg (Hard)	Minimising mass was deemed more necessary than thermal history.
Endurance	2 hrs (Hard)	The total flight time attainable by the batteries at the flight conditions (Abdullah, 2022)
Portability	Man-packable + transportable (Soft)	Wings can be taken off and replaced with small screws making it easy to transport to launch sites (Huckle, 2022).
Manufacture	In house parts with plug and play wings (Soft)	All parts manufacturable in university and plug and play (Section 7)
Launch	Trolley Assisted (Soft)	Edge autonomy catapult delivers the take-off speed necessary (Section 6.1.2).
Autonomy	Fully automated (Soft)	Autonomy removes the need for a pilot thus reducing costs
Failsafe	Autonomous return to home function (-)	As required by the specification.
Wind Speed	20m/s (Hard)	Wind speeds in the UK are rarely as high as 28m/s for an altitude of 120m thus the hard spec is sufficient (Altron, n.d.).
Landing	Runway (Hard)	Landing speed was deemed feasible on a runway of 100m (Section 5.1.2) (Sharma, 2022)
Power	Batteries (-)	As required by the specification (Section 8.3.1)
Maintenance	Replacement components (Soft)	More robust and reliable to replace.
Accessibility	All components (Soft)	All internal components accessible (Huckle, 2022)
Data Transfer	Recorded on board, live transmission (Soft)	Required to be live for the operator to control the aircraft to satisfy CAA regulations (2.4.1) (CAA, 2020). (Section 7.2)
Materials	Sustainable manufacture and recyclability (Soft)	Predominantly made from the sustainable balsa (Alazmi, 2022)

Operation	Night-time and light rain, BVLOS (Soft)	Night vision camera installed to extend operating hours, increasing vaccines delivery frequency. (Abdullah, 2022)
Cost	£2000 (Hard)	Total cost of propulsion and structural (Section 9.6) (Kinirons, 2022) (Abdullah, 2022)
Stability	Meet relevant stability and control regulations (-)	As detailed in section 8.2 and table 8.3.

Figure 2.1 presents the aircraft's mission profile, referred to throughout the report.

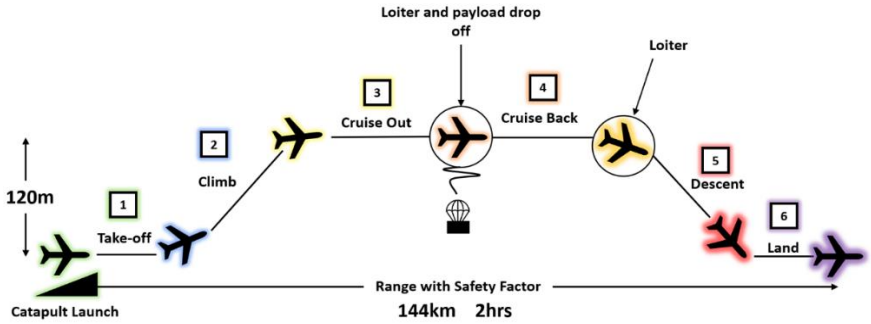

Figure 2.1 - Mission profile

The mission profile above, outlines a return trip from the catapult take-off and runway landing point to deliver to as many remote areas as possible. Additionally, the aircraft was designed with the intention that only one drop would be made from the payload compartment. When the vaccine delivery location is reached, the UAV will decrease in velocity and loiter at the location. From the altitude of 120m, the payload is released once at loiter velocity. There is no need to decrease altitude, as dropping a payload from 120m is deemed acceptable with the use of a parachute, minimising the additional power requirements that would be needed for altitude change (Team 2, 2021). Once the payload is dropped, the UAV will increase back to cruise velocity whilst maintaining an altitude of 120m as will be described further in *Section 7*.

3 Aircraft Design

3.1 Overall Aircraft Layout

Maxine has a high mounted rectangular non-swept flat wing (easily removed for portability as shown in *Figure 3.1),* the landing gear is a tricycle configuration, and the horizontal stabiliser is a high T configuration.

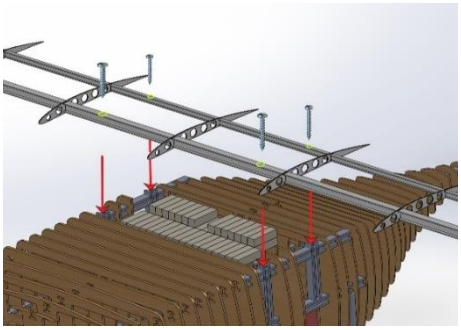

Figure 3.1 – Detachable wing design

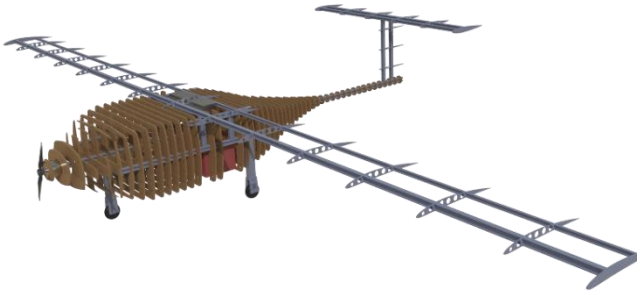

Figure 3.2 – Isometric view of MAXINE

3.2 Internal Components Layout

Figure 3.3 shows the locations of the internal components whilst *Table 3.1* presents information about the internal components, as well as the justification for their positioning.

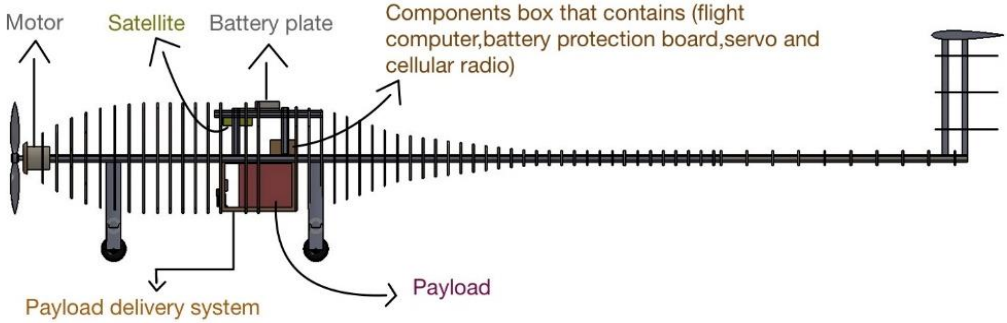

Figure 3.3 - Internal components layout

Table 3.1 - Internal components position justification

Internal component	Position	Justification
Motor	Front of the fuselage	Positioned close to propeller for wiring simplicity resulting in more efficient maintenance and accessibility
Propeller	Front of fuselage	Due to inherent design of UAV.
Batteries	Central location	Placed so that CoG of UAV is in an optimum position calculated by stability and control.
Payload	Central location	Positioned so that when payload is deployed, the CG only moves in the Z direction to make stability and control analysis less complex
Avionics	Positioned below detachable wings.	Positioned to make easily accessible for potential maintenance requirements.
Camera	In front of the landings gear.	Field of view is maximised in this position. Makes emergency piloting of UAV more user friendly.
Cellular radio	Close to exterior of fuselage	This position ensures that signal is as strong as possible.
Satellite radio	Close to exterior of fuselage	This position ensures that signal is as strong as possible.

4 Weight Analysis

4.1 Material selection

Table 4.1 presents the chosen material type for each part of the UAV alongside the materials properties which were later used for computational structural analysis in *Section 7.2* (Alazmi, 2022).

Table 4.1 - Material type and properties for each part

Part	Material	Tensile strength (Mpa)	Youngs modulus (Mpa)	Density (kg/m^3)
Fuselage midsection and nose	Balsa wood	64	10400	270
Wing ribs, empennage, landing gears and fuselage I beams	Magnesium alloy	270	45000	1700
Wing spars	Aluminium alloy	572	71700	2823.35
Fuselage skin	Monokote covering film	270	230	172

4.2 UAV total weight

The total weight for the UAV is 19.2 kg, this is made up of 11.34 kg for propulsion system components and 7.80 kg for the UAV parts (including the payload). The full breakdown for the weights of the individual components and is presented in *Appendix C1 and C2*.

5 Propulsion and Systems

5.1 Propulsion System

Using the drag polars and final weight estimations, the motor and propeller was sized to accommodate the aircraft flying at its maximum velocity of 33.3 m/s. This requires a motor with a power rating of at least 1500W (accounting for inefficiencies). Hence a 2000W brushless DC motor with a KV rating of 580 was chosen for the aircraft, paired with a 12-inch propeller in the “puller” configuration. 12 inches was chosen due to the height constraints of the aircraft and to ensure that the tip speed does not exceed the subsonic regime.

5.2 Avionics Systems

The flight controller chosen is the BeagleBone Blue paired with the Ardupilot operating system due to the versatility and abundance of documentation. Whilst a RaspberryPi was initially considered for the flight controller due to its inherent higher processing power and modularity, it lacked the abundance of built-in

sensors and ports that came with the BeagleBone Blue. The flight controller was paired with a cellular radio for BVLOS communications which provided low-latency, high-bandwidth communication between the aircraft and the ground station. The high bandwidth allowed us to implement a visual verification system with the addition of a high-definition camera, while the low latency connection allowed for real-time remote control of the aircraft. In the unlikely event that the aircraft should lose its cellular connection, a satellite radio was included as a backup. However, it has a significantly lower bandwidth and higher overall latency, therefore it is only used for telemetry and programming changes in mission profiles.

5.3 Battery and Power distribution systems

5.3.1 Battery

Due to the inherently high-power requirement of the motor, the main battery pack is designed with six Li-ion 18650 cells in series to achieve a nominal voltage of 22.2V. This results in a peak current draw of 90A at full throttle and hence necessitates an electronic speed controller rated for at least 100A. To meet the endurance requirements, the battery pack will consist of 216 cells in a 6S18P configuration, resulting in capacity of 2.56kWh. The battery pack was also designed to be modular in design to allow for quick turnover times, therefore two XT60 connectors are used to connect the battery pack to the aircraft. A battery management system (BMS) is added as part of the battery pack which provides over-discharge and over-current protection, and cell charge balancing.

5.3.2 Power distribution

All components of the aircraft are inherently powered by the main battery pack. A Universal Battery Eliminator Circuit (UBEC) is placed between the BMS and the flight computer to regulate the voltage at 9V, and another in-between the communication radios regulated at 5V. An additional backup battery pack in a 2S3P configuration is added to provide redundancy to power avionics and communications systems. This configuration is presented in *Figure 5.1*.

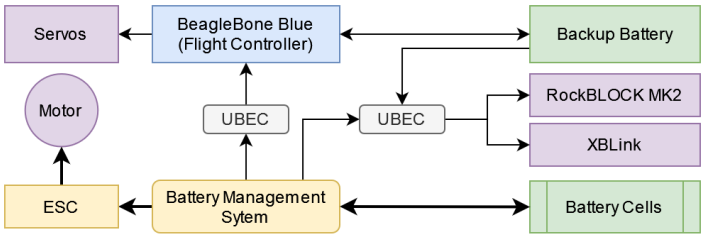

Figure 5.1 - Power distribution wiring diagram showing the connections between the battery pack and system components.

5.4 Payload Release System

This system consists of a box where the payload is fixed in place and protected from detaching and damaging the inner structure. The structure has two inner foam supports to ensure the payload does not oscillate inside and damage the actuators that responsible for release. The system is shown *Figure 5.2*. The release system is activated by a servo motor opening a latch mechanism which opens the trapdoors to release the payload. After release the doors are closed by second servo motor by winding a string on a spool that attaches to the trapdoors (Mazmacs, 2022).

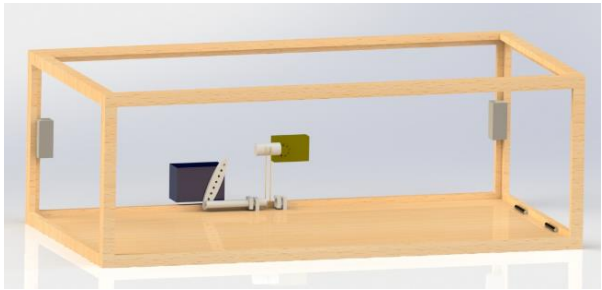

Figure 5.2 - Payload release system

6 Manufacturing and Cost

6.1 Overall Cost Analysis

The aircraft is to be made using balsa wood sheets, magnesium alloy ribs and a combination of aluminium and magnesium alloy spars for the wings and fuselage. The total cost of the raw materials for the aircraft is £274.04 (Kinirons, 2022). The components, however, play a much larger contribution to the total cost with the propulsion system costing £94.48, the battery system costing £605.40 and the avionics £819.89. This brings the overall aircraft cost to a total £1,793.81 *Figures 6.1 and 6.2* show more detailed cost breakdowns.

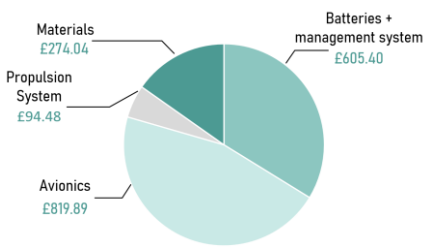

Figure 6.1 - Components costs

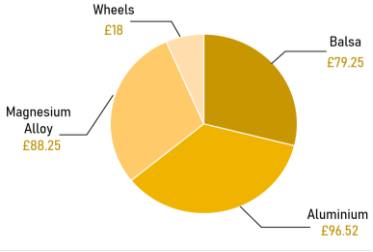

Figure 6.2 - Materials costs

6.2 Production

From an analysis of a UK population density map along with the fact that MAXINE has a safe working range of 72km, all low population density areas across the UK can be covered with 11 separate launch sites. Assuming there will need to be 2 UAVs per launch site so each site has a backup aircraft there will be 22 total UAVs produced in the first production of MAXINE(Craddock, 2022)(Kinirons, 2022).

6.3 Manufacturing

Table 6.1 shows the manufacturing process for each selected material. This corresponds to *Table 4.1* which states what material is selected for each UAV part (Alazmi, 2022).

Table 6.12 - UAV Manufacturing process

Material	Manufacturing process
Balsa wood	Laser cut
Magnesium alloy	University hand tools and milling/lathe techniques
Aluminium alloy	University hand tools and milling/lathe techniques

7 Performance Analysis

7.1 Flight Performance

7.1.1 Wing Performance

The available configurations for the UAV use a cantilever wing or an externally braced wing. The choice of using a cantilever beam wing has been made due to its lower induced drag, and since loadings on this UAV are relatively small, the weight penalty will not be a problem. Furthermore, choosing the cantilever wing allows the ease of manufacturing and the opportunity for quicker assembly and disassembly times. Having considered the options of a high mounted and low mounted wing, the advantages of a high mounted wing outnumber those of a low mounted wing, which include modularity (easily detachable), ground clearance and improved stability. The quarter chord sweep angle does not introduce advantages for the UAV. At its low air speeds, it is quite disadvantageous because it requires higher angles of attack and since it makes the wing longer, in increases weight. Thus, a zero-sweep wing has been chosen. The simulation results show that the optimal aerofoil thickness is around 7-8% of the chord length, with the maximum lift coefficients and lift to drag ratio at a constant angle of attack. After an iterative process in the design, a lift coefficient of 0.405 for the cruise condition has been set. Using this, simulations were run to find the best aerofoil section that meets this lift and the structural criteria, and it was found that NACA 4408 at an angle of attack of 2° is the optimum solution. Non-tapered wings have been chosen because the advantage of protecting the control surfaces from stall outweighs the tapered wing advantage of weight reduction. (Arteni, 2022) (Williamson, 2022) (Eve, 2022)

7.1.2 Flight conditions

Table 7.1 presents the summary of optimum flight conditions, with the proceeding subsections briefly explaining why these are optimum (Sharma, 2022).

Table 7.1: Optimum flight conditions

PHASE	VELOCITY (m/s)	RANGE (m)	TIME (s)	AoA (°) & Climb/Descent	C_L	C_D
1. Take-off	Start: 00.00 End: 16.00	N/A – Catapult launch				
2. Climb	16.00	285.9	16.2	9.5 (AoA) 24.9 (Climb)	1.321	0.1015
3. Cruise out	29.00	71273.5	2458	2.0 (AoA)	0.405	0.0487
4. Cruise back	29.00	71273.5	2458	3.0 (AoA)	0.638	0.0646
5. Descend	11.56	1167.12	116	7 (AoA) 5.16 (Descent)	1.093	0.0829
6. Failure Descent	36.25	628.2	17	-1.5 (AoA) 24.8 (Dive)	0.2146	0.0448
7. Land	11.5	100	17	N/A-Runway landing		
	Total:	144km	1hr24min			

Before breaking down each phase it should be noted that the lift characteristics, C_L, were determined using XFLR5 an aerodynamic analysis tool which employs the use of the vortex and panel methods. XFLR5 allows for the whole aircraft to be modelled (Eve, 2022), except for the landing gear. Thus, in order to determine the full drag coefficient (C_D) the landing gear component of drag was calculated empirically and summated to that outputted by XFLR5 (Williamson, 2022). To summarise the relationship between the lift and drag characteristics the drag polar was determined as shown in *Equation 1*.

$$C_D = 0.04331 + 0.03336{C_L}^2 \quad (1)$$

Where the first term represents C_{D_0}, the zero-lift, and the quadratic term shows k, the lift induced drag coefficients respectively. These were determined by plotting a graph of C_D against ${C_L}^2$ for the final XFLR5 model and taking the equation of the line where the gradient was k and the y-intercept was C_{D_0}.The contribution of C_{D_0} from the landing gear was then added (Sharma, 2022). Time taken and distance travelled was calculated assuming constant velocity and as such used *Equation 2* unless mentioned otherwise (Sharma, 2022).

$$Velocity\ (m/s) = \frac{Range(m)}{Time(s)} \quad (2)$$

Take-off

To satisfy the CAA S51 requirement a velocity of 1.3 times the stall speed, V_s, was used giving 16m/s (CAA, 2009). Where stall speed is determined using the maximum lift coefficient from XFLR5 in *Equation 3*. This velocity is attainable without flaps as market research shows that the 'Edge Autonomy 11kJ pneumatic catapult' was more than capable, offering speeds of up to 25m/s for double MAXINEs maximum take-off weight (MTOW) (Edge Autonomy, 2022). The added benefit of catapult launches minimises battery power demands.

Climb

Assuming straight and level flight (AoA < 13°) *Equation 3* could be used to determine the lift coefficient necessary to achieve 16m/s.

$$v_{stall} = \sqrt{\frac{2W}{\rho S C_{L_{max}}}} \quad (3)$$

Where this was determined at 1.3 and as such a large angle of attack was required of 9.5° as determined by the XFLR5 C_L vs AoA. It also offered an excellent lift to drag ratio to aid endurance *Figure 5.1*.

The climb characteristics were a result of the motor characteristics however using the Hodograph generated (Sharma, 2022), *Figure 6.2*, it is clear that to maintain a velocity of 16m/s a rate of climb (R/C) of 7.4m/s is necessary which produces a climb angle of $24.8°\left(\tan^{-1}\frac{7.4}{16}\right)$.

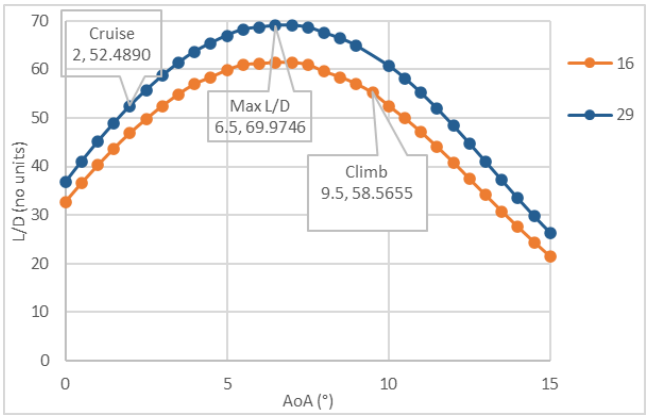

Figure 7.1 - Lift to drag ratio vs angle of attack

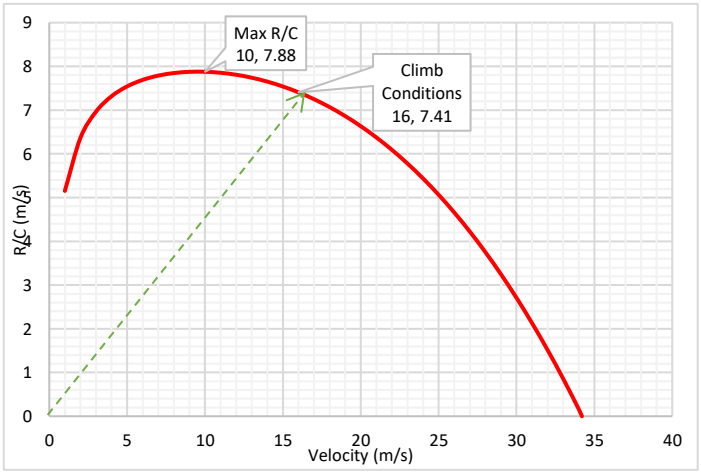

Figure 7.2 - Rate of climb vs velocity

Cruise out

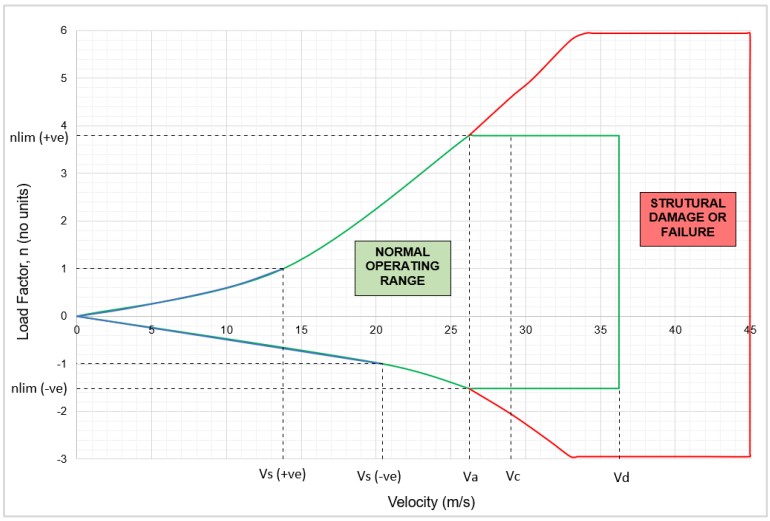

Figure 7.3 - Load factor vs velocity

The cruise speed, V_c, of 29m/s was determined by using a structurally optimum velocity found when constructing the V-n diagram, *Figure 7.3* (Sharma, 2022). This velocity is within the normal operating range. To attain this velocity, a lift coefficient of 0.4047 was calculated, using *Equation 4*.

$$v = \sqrt{\frac{2W}{\rho S C_L}} \tag{4}$$

When using the relationship of the C_L and AoA, 2° was determined as necessary to achieve this. The compromise at cruising at 29m/s is a lower lift to drag ratio shown in *Figure 7.1*, however a lower cruise velocity is not structurally manoeuvrable.

Cruise back

A drop of the payload meant the XFLR5 model was altered to be 3kg lighter. This meant to achieve the same velocity, 29m/s, a C_L of 0.638 was required, using *Equation 4*, and as such the angle of attack of the aircraft is increased to 3° (Sharma, 2022).

Descend & Engine Failure Descent

CAA requirements dictate that the descent velocity of the aircraft must be at least $1.3V_{stall}$ (CAA, 2009). Using the reduced mass after payload deployment the stall speed is reduced to 8.89m/s, using *Equation 3*. To obtain the 11.56m/s ($1.3V_{stall}$) an AoA of 9.5° is required to sufficiently slow the aircraft down. The descent angle was then determined by use of the rate of descent *Equation 5* (Sharma, 2022).

$$\theta_D = \sin^{-1}\frac{v}{V} \tag{5}$$

Where V is 11.56 and v is determined using *Equation 6:*

$$v = V\sin\theta_D = \sqrt{\frac{2W}{\rho S C_L}} \times \frac{C_D}{C_L} \tag{6}$$

As this analysis assumed straight and level flight ideally the aircraft should descend at these conditions even if the engine were to fail however, testing the diving abilities of the aircraft in a worst-case scenario it was found that the dive angle at the dive speed shown on *Table 7.1* was found to be 24.8 degrees using *Equation 5.*

Land

Assuming the aircraft lands at its descent speed (11.56m/s) and experiences constant deceleration upon landing a sloped 100m runway was deemed optimal using *Equations 7 and 8*:

$$s = \frac{u+v}{2}t \ (\mathbf{7}) = \frac{11.56+0}{2}t = 5.78t, \qquad 100 = 5.78t \ \ \therefore t = 17.3s$$

$$v = u + at \ (\mathbf{8}) = 11.56 + 17.3a, \qquad 0 = 11.56 + 17.3a \ \ \therefore a = -0.67m/s^2$$

The deceleration is low (less than $1m/s^2$), ensuring a gentle stop.

7.2 Structural Performance

Extensive structural integrity investigations of the wings were carried out using Computational Structural Dynamics (using Abaqus FEA) to determine the maximum tip deflection and stress distributions at different operating conditions. A conservative aerospace safety factor of 1.5 was applied, after which the wing was still shown to be below the limits of maximum stress and therefore not be at risk of failure. A different safety factor was applied for the tip deflection criteria; if the tip deflection was <10% then that was considered acceptable. *Table 7.2* displays this data (Nixon, 2022).

Table 7.2 - Wing Abaqus analysis

Loading scenario	Tip deflection (mm)	Percentage tip deflection (%)	Maximum Von Mises stress (MPa)	Stress safety factor
Cruise	49.59	2.80	55.61	9.05
Maximum load factor	143.00	8.06	160.50	3.13

The yield strength of the aluminium alloy used is 503 MPa. As is shown in *Table 7.2*, the minimum safety factor, for the worst-case scenario, is 3.13. Therefore, the wing is considered to be suitable for all flight as described in the V-N diagram. The tip deflection and maximum Von Mises stress at the maximum load factor are 143mm and 160MPa (see *Appendix E*). The maximum stress locations for the main are rear spar are at the innermost rib, where they are fixed in place (encastre boundary condition; prevents displacement and rotation).

The landing gear configuration chosen was a fixed tricycle landing gear. This was chosen because there was a lack of space for retractable landing gear, it required the least amount of skill to land, and it was the cheapest option. After a CSD analysis, the maximum stress at landing was 2.15 MPa while the maximum tensile strength was 220 MPa. In addition, it was observed that the strut would not buckle as it would fail before that point, since the maximum stress at buckling was 698 MPa. Furthermore, the displacement caused by the friction of the wheel with the ground was evaluated to observe if it could affect the stability of the aircraft. It was found that the horizontal displacement was 0.003 mm which would be small enough to be neglected during landing. The main criteria for the fuselage reinforcements, was to decide the position of the ribs, the desired shape of the fuselage and the locations of concentrated stress, therefore regions like the landing gear or the wing connections to the fuselage were strategic places to locate the ribs. It was found that 100 mm distance between the ribs, maintains the shape and the integrity of the fuselage. The displacement of the tail when applying a lateral load of 3N was found to be 3 cm relative to the fuselage axis. However, the model did not consider the resistance of the tail due to the volume of air that needs to be moved, which means that the displacement should in fact be smaller. Another CSD analysis was performed to evaluate the integrity of the structure at landing. It was found that the maximum stress at landing was 123.8 MPa while the maximum tensile strength of magnesium was 220 MPa which results in a safety factor of 1.78. Therefore, according to the conservative aerospace safety factor mentioned before, the fuselage structure can be considered as suitable for flight.

8 Control

8.1 Control Sizing

The required horizontal stabiliser dimensions were initially determined using Class I longitudinal stability analysis (Roskam, 1985). A minimum requirement of 10% static margin was set, which was achieved by setting the horizontal stabiliser dimensions to 0.2m chord, 1m span and 0.2m^2 area.

Figure 8.1 shows the longitudinal x plot, with the impact of horizontal stabiliser area on aerodynamic centre and centre of mass, the latter determined using the CAD model. The horizontal tail later moved further aft, increasing the static margin from 10.4% to 22.2%, the latter determined using XFLR5 instead of the Class I methods. Due to the greater importance of stability over manoeuvrability of the aircraft, this was determined acceptable, and the horizontal tail area was not reduced to minimise impact on the design. The vertical stabiliser area was initially determined using Class I lateral stability analysis (Roskam, 1985).

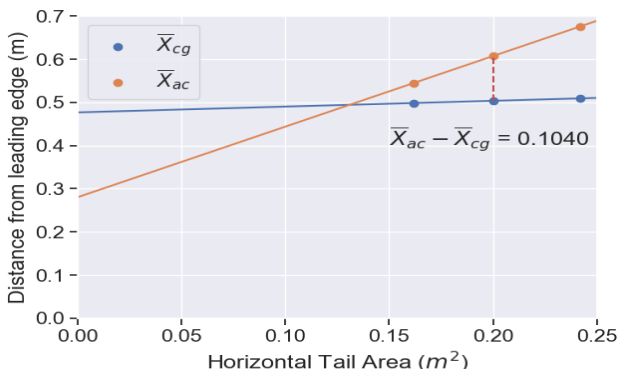

Figure 8.1 - Distance from leading edge vs horizontal tail area

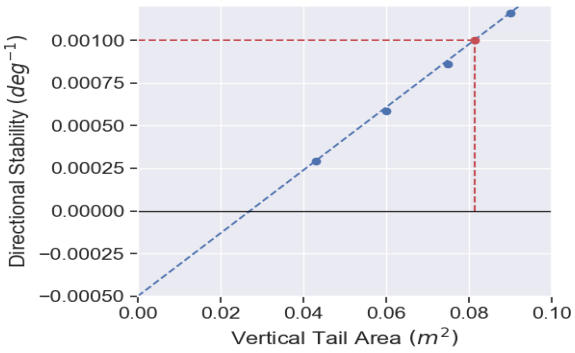

Figure 8.2: Directional stability vs vertical tail area

From Roskam (Roskam, 1985), the minimum yaw rate with sideslip angle derivative, C_{n_β} should be $0.0010 deg^{-1}$ i.e., with sideslip, the aircraft should have the tendency to correct its yaw rate. A lateral x plot was used, shown in *Figure 8.2*, to determine the required vertical stabiliser area. Unlike the horizontal

stabiliser, the chord and span were not increased proportionally and therefore additional XFLR5 simulations were performed to determine the change in coefficient of lift against sideslip for the vertical stabiliser. The vertical stabiliser dimensions were set to 0.550m by 0.150m giving an area of 0.0825m^2. As with the horizontal stabiliser, the vertical stabiliser was not reduced in size when the vertical stabiliser was moved aft. Both the stabiliser dimensions were compared to empirical data from literature, showing good coherence with Raymer (Raymer, 1999) which suggested a vertical stabiliser area of 0.0864m^2 and a horizontal stabiliser area of 0.166m^2. The dimensions of the control surfaces for the final design iteration are given in *Table 8.1*.

Table 8.1 - Final design iteration dimensions

Surface	Chord length (m)	Span (m)	Area (m^2)
Wing	0.313	4.07	1.27391
Horizontal Stabiliser	0.2	1	0.2
Vertical Stabiliser	0.15	0.547	0.08205
Aileron	0.0939	1.01	0.09484
Rudder	0.045	0.512	0.02304
Elevator	0.06	0.97	0.0582

8.2 Flight Stability

Table 8.2 - Static Stability Acceptability Criteria

Forces and Moment		Perturbed Variables							
		u	v	w	Beta	Alpha	p	q	r
Forces	XA + XT	True							
	YA + YT		True						
	ZA + ZT			True					
Moments	LA + LT				True		True		
	MA + MT	True				True		True	
	NA + NT				True				True

Table 8.2 presents the criteria for the aircraft to be statically stable, which demonstrates that the aircraft is statically stable, since the conditions for acceptability are all met. (Hawes, 2022) (Kalathurvadyar, 2022)

Table 8.3 presents the flight stability performance for different flight characteristics and determines whether these are acceptable under the applicable flight regulations.

Table 8.3 - Flight Characteristics

Characteristic	Applicable Regulation(s)	Value
Roll Mode Performance	Aircraft must be able to bank 60 degrees (e.g., to reverse a 30-degree bank to –30 degrees) within 5 seconds (CAA, 2009)	60 degrees roll possible within 2.21 seconds at all mission stages (Cradock, 2022).
Landing in Crosswind	No specific value, however, the maximum crosswind landing value must be investigated and provided in the operators' manual (CAA, 2009)	Maximum crosswind landing velocity is 5m/s, corresponding to a crosswind angle of 22.3 degrees during approach, limited by having no motorised steering and the maximum crab angle being 28 degrees (Cradock, 2022).
Dynamic Longitudinal Stability	For all flight stages: $\zeta_P \zeta_P > 0.04$ *For climb and cruise:* $0.3 < \zeta_{SP}$ <For climb and cruise: $0.3 < \zeta_{SP} < 2.0$ *For descent:* $0.35 < \zeta_{SP}$ <For descent: $0.35 < \zeta_{SP} < 1.3$ Where $\zeta = damping\ ratio;\ SP = short\ period\ response;\ P = phugoid\ response$ $\zeta =$ damping ratio; SP = short period response; P = phugoid response (Nelson, 1998)	All requirements met at all flight stages (Cradock, 2022).
Spiral Mode Stability	For all flight conditions: $$L_\beta N_r - N_\beta L_r > 0$$ Where: $L_\beta =$ roll moment derivative with sideslip $N_r =$ yaw moment derivative with yaw rate	All requirements met at all flight stages (Cradock, 2022).

	N_β = yaw moment derivative with sideslip L_r = roll moment derivative with yaw rate (Roskam, 1985)	
Dutch Roll Mode Stability	For all flight stages: $\zeta\zeta \geq 0.08$ For climb and cruise: $\omega_n\omega_n \geq 0.4$ For descent: $\omega_n\omega_n \geq 1.0$ Where ζ = damping ratio; ω_n = natural frequency *For Dutch roll mode* (Nelson, 1998)	All requirements met at all flight stages (Cradock, 2022).
Longitudinal Controllability and Trim	Acceptability: Maximum Elevator Deflection (Roskam, 1985)*:* $\lvert\delta_e\rvert < 25°$ Angle of Attack, for established flight conditions ($C_{L\_Initial}$ and C_{L_End})*:* $\alpha < \alpha_{Stall}$ Tail Stall: Tail stall locus must not within the boundaries of the trim triangle	Elevator Deflection to Trim: $\delta_e \approx 0°$ Maximum Deflection: $\lvert\delta_e\rvert = 10°$ Angle of Attack: $C_{L\_Initial}$: $0.5° < 15°$ C_{L_End}: $0° < 15°$ Tail Stall locus positioned outside the boundaries of the aircraft trim triangle (Hawes, 2022) All requirements met (Hawes, 2022).
Directional and Lateral Controllability and Trim	Acceptable Criteria: Sideslip angle: $\beta < 5°$, for drag $\beta < 12°$, for directional stability Aileron deflection: $\lvert\delta_a\rvert < 25°\lvert\delta_a\rvert < 25°$ Rudder deflection: $\lvert\delta_r\rvert < 25°\lvert\delta_r\rvert < 25°$ (Roskam, 1985)	Sideslip angle (β): $4.48° < 5°$, for drag $< 12°$, for directional stability Aileron deflection ($\lvert\delta_a\rvert$): $0.32° < 25°$ Rudder deflection ($\lvert\delta_r\rvert$): $6.94° < 25°$ (Kalathurvadyar, 2022)
Minimum Control Speed	Acceptable Criteria: $V_a < V_{mc} < 1.2V_s V_a < V_{mc} < 1.2V_s$ *Where:* V_a Where: V_a = approach velocity for landing V_s = stall speed (Roskam, 1985)	$11.56\ m/s < V_{mc} < 14.64\ m/s$ Where: V_a = 11.56 m/s (from *Table 7.1*) V_s = 12.2 m/s (from section 6.1.2) Verification found in (Kalathurvadyar, 2022)

9 Conclusion

After many cycles in the development process of this UAV, in which changes have been made to all aspects of the system to optimise its performance, from the location and sizing of the control surfaces and the controlling algorithm that inflicts a very stable flight configuration, the structural integrity of the wing which has undergone many CSD simulations to confirm its capability of resisting the aerodynamic loads, the internal layout of the UAV to maximise the space available for the important payload, and the appropriate quantity of batteries to be used such that the UAV reaches its targets safely but without compromising the payload weight.

The result is a drone that, once manufacturing begins, will be an efficient and cost-effective way of distributing vaccines to the most remote places, where it is not feasible to use any other method of transportation.

References

18650 UK Ltd, 2020. *Samsung 35E - 18650 Battery.* [Online]
Available at: https://www.18650.uk/samsung-35e---18650-battery
[Accessed 19 10 2021].

Abdullah, I., 2022. *Individual Report,* s.l.: s.n.

Alazmi, H., 2022. *Team member individual report ,* s.l.: s.n.

Altron, n.d. *Wind Loading Data.* [Online]
Available at: https://www.altron.co.uk/wind_loading_data.html.

Bronz, M., Moschetta, J.-M. & Hattenberger, G., 2012. *Multi-Point Optimisation of a Propulsion Set as Applied to a Multi-Tasking MAV,* Braunschweig: IMAV.

CAA, 2009. *CAP 482.* Gatwick: The Stationery Office.

CAA, 2020. *CAP 722: Unmanned Aircraft System Operations in UK Airspace - Guidance.* [Online]
Available at: https://publicapps.caa.co.uk/modalapplication.aspx?appid=11&mode=detail&id=415

Corrigan IV, E. K., 2007. *Survey of Small Unmanned Aerial Vehicle Electric Propulsion System,* Dayton: University of Dayton.

Cradock, B., 2022. *Team member individual report,* s.l.: s.n.

Cutler, C., 2015. *Dihedral Keeping Your Wings Level.* [Online]
Available at: https://www.boldmethod.com/learn-to-fly/aerodynamics/dihedral-keeping-your-wings-level/
[Accessed November 2021].

Dündar, Ö., Bilici, M. & Ünler, T., 2020. Design and performance analyses of a fixed wing battery VTOL UAV. *Engineering Science and Technology, an International Journal,* 23(5), pp. 1182-1193.

Eve, L., 2022. *Individual team member report,* s.l.: s.n.

Gong, A. & Verstraete, D., 2017. *Experimental Testing of Electronic Speed Controllers for UAVs.* Sydney: University of Sydney.

GreenRiverside, n.d. *Energy Efficient Motors.* [Online]
Available at: http://www.energydepot.com/RPUcom/library/MISC003.asp
[Accessed 2021].

Gundlach, J., 2012. *Designing Unmanned Aircraft Systems: A Comprehensive Approach.* Virginia: American Institute of Aeronautics and Astronautics, Inc.

Hawes, M., 2022. *Team member individual report,* s.l.: s.n.

Jahnavi & Avinash, 2014. Aircraft Design and Weight Estimation Nomenclature. *Global Journal of Researches in Engineering,* 14(4), pp. 35-39.

Janes Group UK, 2001. UAVs. In: *Jane's All the World's Aircraft.* Coulsdon: Janes Group UK, pp. 3-293.

Kalathurvadyar, T., 2022. *Team member individual report,* s.l.: s.n.

Kinirons, J., 2022. *Team member individual report,* s.l.: s.n.

Landolfo, G., 2008. *Aerodynamic and Structural Design of a Small Non-planar Wing UAV,* Dayton: University of Dayton.

laxman, 2020. *Empty Weight Fraction Estimation.* [Online]
Available at: https://wingsofaero.in/calculator/empty-weight-fraction-estimation-laxman/
[Accessed 19 10 2021].

Mazmacs, E., 2022. *Team member individul report,* s.l.: s.n.

Nelson, R. C., 1998. *Flight Stability and Automatic Control.* s.l.:s.n.

Nixon, D., 2022. *Team member individual report,* s.l.: s.n.

Onslow, D., 2020. *2-Way Radio Range: How Far Can Two-Way Radios Communicate.* [Online]
Available at: https://www.intercomsonline.com/2-way-radio-range-how-far-can-two-way-radios-communicate
[Accessed November 2021].

Raymer, D., 1999. *Aircraft design: A conceptual approach, American institute of astronautics.* s.l.:s.n.

Raymer, D. P., 1992. *Aircraft Design: A Conceptual Approach.* Washington D.C.: American Institute of Aeronautics and Astronautics, Inc.

Roskam, J., 1985. *Airplane Design Part 1: Preliminary Sizing.* Ottawa: Roskam Aviation and Engineering Corporation.

Russell, J. B., 1996. *Perfomance and Stability of AIrcraft.* Oxford: Butterworth-Heinemann.

Scholz, D., 2015. *Aircraft Design.* Hamburg: University of Hamburg.

Sharma, A., 2022. *Team member individual report,* s.l.: s.n.

Team 2, 2021. *Team 2 Preliminary Report,* Leeds: University of Leeds.

Torenbeek, E., 2013. *Advanced Aircraft Design: Conceptual Design, Analysis and Optimization of Subsonic Civil Airplanes.* 1st ed. Hoboken: John Wiley & Sons.

Williamson, M., 2022. *Individual team member report,* s.l.: s.n.

Appendix B – Aircraft Detailed Design Views

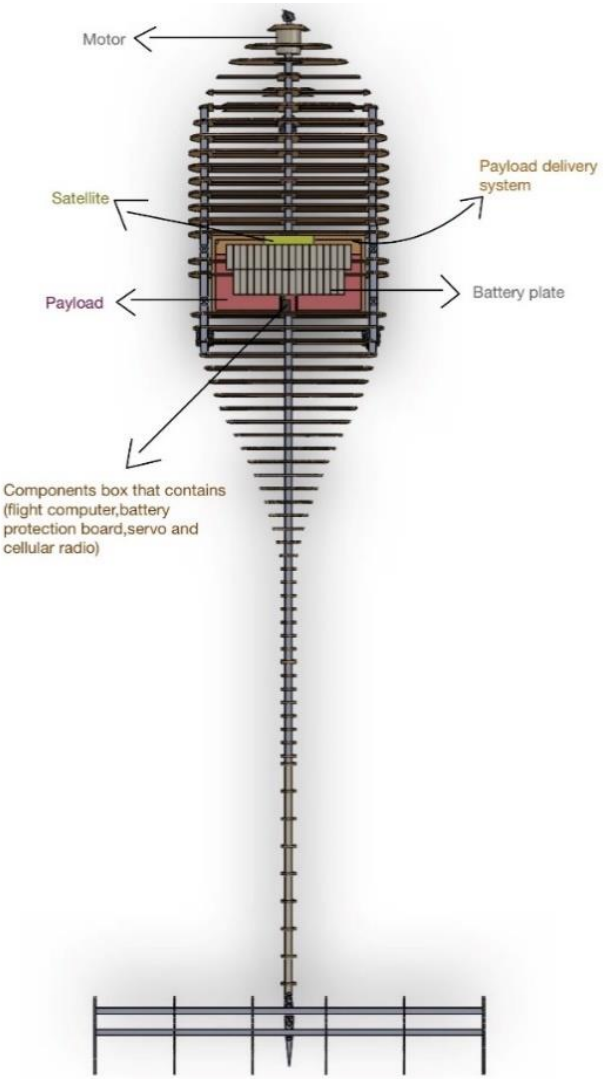

Figure B1 - Top view diagram showing the internal components location

Appendix C Weight analysis

Table C1 - Weights of the Systems Components

	Item	Qty	Unit Weight (g)	Total Weight (g)
A	Beagleboard Blue (Flight computer)	1	36.0	36.0
	RockBLOCK MK2 (Satcom)	1	72.0	72.0
	XBLink (Cellcom)	1	74.0	74.0
	XBCam (Camera)	1	14.5	14.5
	Control Surface Servos	4	10.3	41.0
	Payload Delivery Servos	2	27.0	54.0
	Matek Micro BEC	2	2.0	4.0
B	18650 Battery Cell	222	48.7	10,813.6
	Battery Management System	1	50.0	50.0
P	Motor	1	331.0	331.0
	Propeller	1	20.0	20.0
	Electronic Speed Controller	1	128.0	128.0
			TOTAL WEIGHT (g)	11,638.1

Table C2 - Weights of the UAV parts

Part	Weight (kg)
Fuselage	2.43
Wing	2.33
Tail	0.49
Landing gears	1.12

Appendix D Cost & Production numbers

Table D1 - Costs of the Systems Components

	Item	Qty	Unit Price	Subtotal
A	Beagleboard Blue (Flight computer)	1	£ 60.23	£ 60.23
	RockBLOCK MK2 (Satcom)	1	£ 205.50	£ 205.50
	XBLink	1	£ 500.00	£ 500.00
	Control Surface Servos	4	£ 5.22	£ 20.87
	Payload Delivery Servos	2	£ 11.30	£ 22.59
	Matek Micro BEC 6-60V 5V/9V/12V Adjustable	2	£ 5.35	£ 10.70
B	18650 Battery Cell	222	£ 2.60	£ 577.20
	Battery Management System	1	£ 43.80	£ 43.80
P	Motor	1	£ 45.59	£ 45.59
	Propeller	1	£ 20.00	£ 20.00
	Electronic Speed Controller	1	£ 28.89	£ 28.89
	TOTAL COST (£)			£ 1,535.37

Table D2 - Materials cost breakdown

Material	Cost
5mm Balsa	£79.25
Aluminium Beams	£88.25
Magnesium Alloy Beams	£41.68

Magnesium Alloy Ribs	£6.82
Landing Gear Shafts	£8.27
Landing Gear Wheels	£18.00
Total materials cost	£242.28

Appendix E Structural performance

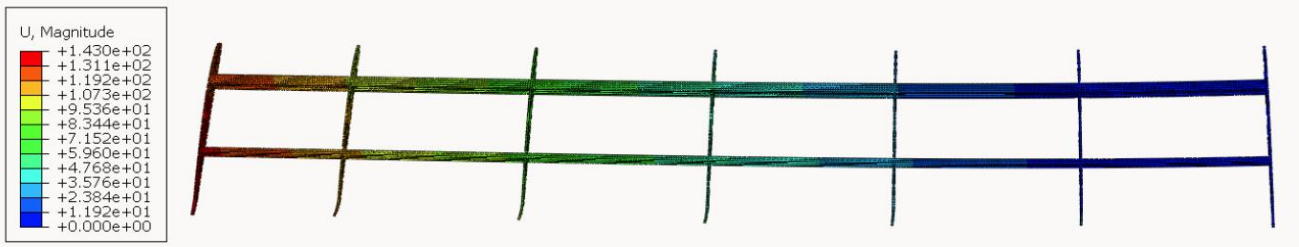

Figure E1 - Wing displacement results from Abaqus

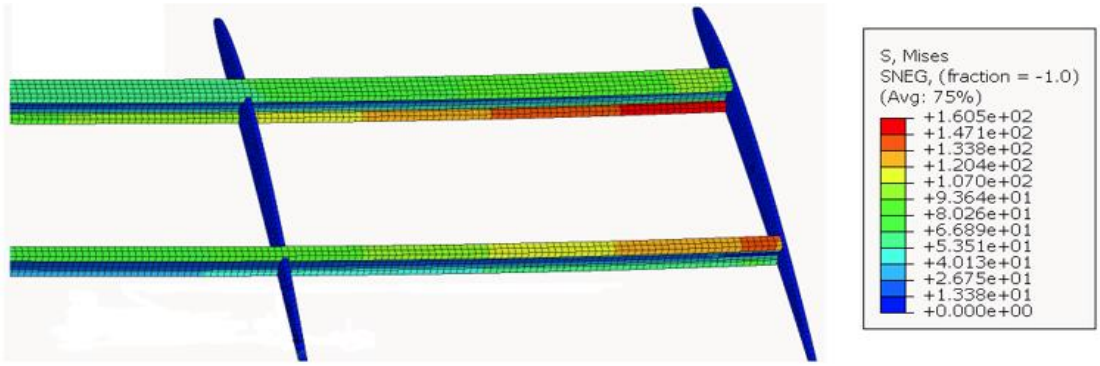

Figure E2 - Wing stress results from Abaqus

Appendix F propulsion system

Figure F1 - motor used for the UAV

Figure F2 - Propeller used for the UAV

Appendix G Dimensioned Drawings